On the time development of dispersion in electroosmotic flow through a rectangular channel

Suvadip Paul · Chiu-On Ng

Department of Mechanical Engineering, The University of Hong Kong,
Pokfulam Road, Hong Kong, China

Abstract

This is an analytical study on the time development of hydrodynamic dispersion of an inert species in electroosmotic flow through a rectangular channel. The objective is to determine how the channel side walls may affect the dispersion coefficient at different instants of time. To this end, the generalized dispersion model, which is valid for short and long times, is employed in the present study. Analytical expressions are derived for the convection and dispersion coefficients as functions of time, the aspect ratio of the channel, and the Debye–Hückel parameter representing the thickness of the electric double layer. For transport in a channel of large aspect ratio, the dispersion may undergo several stages of transience. The initial, fast time development is controlled by molecular diffusion across the narrow channel height, while the later, slower time development is governed by diffusion across the wider channel breadth. For a sufficiently large aspect ratio, there can be an interlude between these two periods during which the coefficient is nearly steady, signifying the resemblance of the transport to that in a parallel-plate channel. Given a long enough time, the dispersion coefficient will reach a fully-developed steady value that may be several times higher than that without under the side wall effects. The time scales for these periods of transience are identified in this paper.

Keywords Taylor dispersion · Electroosmotic flow · Generalized dispersion model

1 Introduction

Channels in modern microfluidic devices and MEMS (microelectromechanical systems), made by micromachining, are commonly rectangular in cross section. The aspect ratio of the channel, viz. the ratio of the breadth to the height of the channel, is typically larger than unity. For a sufficiently large aspect ratio, the side walls may be ignored as far as the flow is concerned. The velocity profile of flow through a rectangular channel of very large aspect ratio is practically not different from that through a parallel-plate channel of the same height. This argument cannot be extended, however, to hydrodynamic dispersion. It is well known in the literature that dispersion in a rectangular channel does not necessarily reduce to that in a parallel-plate channel as the aspect ratio tends to infinity.

The focus of this paper is on solute dispersion in flow driven by electroosmosis in a channel of rectangular cross section. Electroosmotic flow is essentially caused by the viscous motion of free charges in the fluid when subjected to an applied electric field along the channel. The free charges owe their presence to the formation of an electric double layer (EDL) near a charged surface bounding the channel. Electroosmotic flow is known to be more advantageous than pressure-driven flow as its flow rate is less restricted by the minute transverse dimensions of a microchannel. While there already exist some studies on hydrodynamic dispersion in electroosmotic flow, a central question remains unanswered thus far: how does the dispersion in electroosmotic flow evolve with time under the effect of the channel side walls? Let us briefly review the literature, and explain the motivation of our study as follows.

The issue regarding the effects of side walls on mass transport was addressed long time ago. Three-dimensional laminar dispersion in gravity- or pressure-driven flow in open and closed rectangular conduits was analyzed by Doshi et al. [1]. They showed that the dispersion coefficient does not reduce to that in a channel without side walls. They arrived at an important conclusion: as the aspect ratio of the rectangular channel tends to infinity, the effect of vertical and horizontal gradients of velocity and concentration is additive. The large-time asymptotic steady dispersion coefficient for a channel of infinite aspect ratio is found in their analysis to be about eight times the one obtained by neglecting the side walls. Takahashi and Gill [2] further studied three-dimensional laminar dispersion in rectangular

conduits with transverse flow with possible applications in hydrodynamic chromatography. They also found that side walls may not be neglected even when the aspect ratio is very high.

Dispersion in flow driven by pressure or electrokinetics in microchannels has been receiving attention only in recent years. Using a thin double-layer approximation, Zholkovskij et al. [3] investigated electroosmotic dispersion for arbitrary geometry of the microchannel cross section. Dutta and Leighton [4] studied dispersion in large-aspect-ratio microchannels for open channel liquid chromatography. Hydrodynamic dispersion in different cross sectional geometries was then studied by Zholkovskij and Masliyah [5] under combined pressure and electrically driven flows. Ajdari et al. [6] explored the effect of cross-sectional shape on hydrodynamic dispersion in shallow microchannels. They investigated the role of channel side walls on axial dispersion in electrokinetically and pressure-driven chromatographic systems. The influence of the geometry of microchannel on solute dispersion in pressure-driven flow was investigated by Dutta et al. [7]. Considering small zeta potentials, Dutta [8, 9] studied electrokinetic transport through rectangular channels and examined the role of side walls. He also presented an analytical theory, which was valid for large aspect ratio, for estimating the solute dispersion by decoupling the effects of vertical and horizontal velocity gradients in the channel. Vikhansky [10] presented an analytical analysis, based on the lubrication approximation, for dispersion in a microchannel of a slender shallow cross-section. The effect of channel side walls on the transport of neutral samples through rectangular conduits was investigated by Dutta [11] under pressure-driven flow and small zeta potential conditions.

Due to the complexity arising from the presence of side walls, there are some indirect approaches to quantify the effect of side walls on the dispersion. One such approach is to ignore the gradients in the streamline velocity across the narrower dimension of the channel. Motivated by the work of Doshi et al. [1], a few attempts [8, 9] have been made to estimate the effect of the channel side walls by treating the rectangular channel of high aspect ratio as a parallel-plate geometry with a one-dimensional velocity profile obtained by depth averaging of the velocity. The overall dispersion in the rectangular channel may then be evaluated by simply adding the dispersivity in a parallel-plate device to this contribution due to the side regions. This treatment is, however, strictly valid for infinitely wide rectangular conduits

and can only predict the dispersivity of sample slugs in the large aspect ratio limit. Desmet and Baron [12] showed that the additional band broadening due to the side regions in a rectangular conduit could be quantified by assuming the presence of a pseudo-stationary layer on the channel side walls. In spite of a large number of investigations, there still remain uncertainties concerning the effects of side walls. Most of the attempts thus far regarding these effects have been limited to the steady state valid at large times. A theory is yet to be developed to capture the dependence on time of the dispersivity in a rectangular channel under the effects of side walls.

In this work, we tackle the problem of transport in a rectangular channel where the flow is driven purely by electroosmosis, which is a realistic model of hydrodynamic chromatography. The objective is to determine how the hydrodynamic dispersion is affected by the side walls as a function of time. In this regard, the work of Doshi et al. [1], who considered gravity- or pressure-driven flow, is extended to the present problem of transport in electroosmotic flow. The asymptotic steady-state transport coefficients have been derived by Zholkovskij et al. [3] and Dutta [8]. Here we are going to derive the transport coefficients as functions of time, covering these asymptotic steady values at large times. To this end, we shall employ the generalized dispersion model [13], which is valid for all times, to derive expressions for the convection and dispersion coefficients as explicit functions of time, the EDL thickness, and the channel aspect ratio. For comparison, transport coefficients for flow through a parallel-plate channel are also derived. We shall examine the side wall effects by looking into how the ratio of the dispersion coefficients for the two geometries will change with time and other parameters.

The article is organized as follows. In Sec. 2, flow through a rectangular channel is considered. After problem formulation in Sec. 2.1, the generalized dispersion model is introduced in Sec. 2.2. Transport coefficients for a rectangular channel are determined in Sec. 2.3, and then some approximation of the dispersion coefficient is considered in Sec. 2.4. This is followed by analysis on the transport in a parallel-plate channel in Sec. 3. The consistency of the present model with the theory of Desmet and Baron [12] is checked in Sec. 4. Finally, discussions and results are presented in Sec. 5, while Sec. 6 contains our concluding remarks.

2 Flow and transport in a rectangular channel

2.1 Problem formulation

As shown in Fig. 1(a), we consider a two-dimensional rectangular microchannel of height $2h$ and width $2b$, which is filled with an aqueous liquid with free ions. The aspect ratio of the channel is denoted by $\lambda = b/h$. The length of the rectangular channel is much greater than its transverse dimensions, b, h, so that the end effects can be neglected. Cartesian coordinates are used here with the z-axis along the flow, and the x- and y-axes being respectively in the horizontal (spanwise) and vertical (height) directions. The boundaries are situated at $x = \pm b$ and $y = \pm h$. An axial electrical field E is imposed on the system resulting in electroosmotic flow through the channel. See, for examples, Refs. [14, 15] for details about the basic mechanisms of electroosmotic flow.

The fluid is assumed to be isothermal, Newtonian and incompressible. In the absence of pressure gradient, the momentum equation for the electroosmotic velocity $u(x, y)$ can be written as

$$\mu \left(\frac{\partial^2 u}{\partial x^2} + \frac{\partial^2 u}{\partial y^2} \right) + \rho_e(x, y) E = 0, \tag{1}$$

where u is the fluid velocity, ρ and μ are the fluid density and the dynamic viscosity, respectively, and ρ_e is the electric charge density. Equation (1) is subject to no-slip boundary conditions at the walls (i.e., $u = 0$ at $x = \pm b$ and $y = \pm h$).

For simplicity, a uni:univalent electrolyte in the fluid is considered. Assuming that the flow and electric fields are not strong enough to disturb the EDL significantly from equilibrium, we may invoke the static Boltzmann distribution for the charge density:

$$\rho_e = -2ezc_0 \sinh \left(\frac{ze\psi}{RT} \right), \tag{2}$$

where ψ is the electrokinetic potential, c_0 is the ion concentration far from the charged-walls, z is the valence of the ions in the carrier liquid, e is the electron charge, R is the Boltzmann constant, and T is the absolute temperature.

The EDL potential ψ can be described by the following Poisson equation:

$$\frac{\partial^2 \psi}{\partial x^2} + \frac{\partial^2 \psi}{\partial y^2} = -\frac{\rho_e}{\epsilon}, \tag{3}$$

where ϵ is the permittivity of the liquid medium.

Combination of Eq. (2) and (3) gives rise to the following Poisson–Boltzmann equation:

$$\frac{\partial^2\psi}{\partial x^2}+\frac{\partial^2\psi}{\partial y^2}=\frac{2ezc_0}{\epsilon}\,\sinh\left(\frac{ze\psi}{RT}\right). \tag{4}$$

If the electric potential is sufficiently small, typically $\psi \le \psi_0 \approx 25\text{mV}$, the Debye–Hückel approximation can be applied to Eq. (4), resulting in the following linear equation:

$$\frac{\partial^2\psi}{\partial x^2}+\frac{\partial^2\psi}{\partial y^2}=\frac{2e^2z^2c_0}{\epsilon RT}\psi=k^2\psi, \tag{5}$$

where $k=\sqrt{2e^2z^2c_0/\epsilon RT}$ is the reciprocal of the Debye length (a length scale for the thickness of the EDL), also known as the Debye–Hückel parameter.

The boundary conditions for (5) are prescribed by the wall potentials. For the present study, we consider a uniform wall potential ζ on the channel walls i.e., $\psi=\zeta$ at $x=\pm b$ and $y=\pm h$.

Now Eq. (5) with the prescribed boundary conditions yields the following solution

$$\psi \;=\; \zeta\frac{\cosh(ky)}{\cosh(kh)}+\zeta\frac{4}{\pi}\sum_{n=0}^{\infty}\frac{(-1)^n}{2n+1}\frac{k^2}{\beta_n^2}\frac{\cosh(\beta_n x)}{\cosh(\beta_n b)}\cos(\alpha_n y), \tag{6}$$

where

$$\alpha_n=(2n+1)\pi/2h, \qquad \beta_n=(\alpha_n^2+k^2)^{1/2}. \tag{7}$$

From Eqs. (1), (3) and (5) we have

$$\frac{\partial^2 u}{\partial x^2}+\frac{\partial^2 u}{\partial y^2}=\frac{\epsilon E}{\mu}k^2\psi. \tag{8}$$

By inspection of Eqs. (5) and (8), one can readily find that the solution of Eq. (8) satisfying the no-slip boundary conditions on the channel walls is simply given by $u=(\epsilon E/\mu)(\psi-\zeta)$, or

$$u(x,y)=U\left[1-\frac{\cosh(ky)}{\cosh(kh)}\right]-U\frac{4}{\pi}\sum_{n=0}^{\infty}\frac{(-1)^n}{2n+1}\frac{k^2}{\beta_n^2}\frac{\cosh(\beta_n x)}{\cosh(\beta_n b)}\cos(\alpha_n y), \tag{9}$$

where $U=-\epsilon E\zeta/\mu$ is the Helmholtz–Smoluchowski velocity, which is the plug flow electroosmotic velocity in the limit of an infinitely thin EDL.

The velocity averaged over the cross section of the channel is given by

$$\begin{aligned} u_m &= \frac{1}{4bh}\int_{-h}^{h}\int_{-b}^{b} u(x,y)dxdy \\ &= U\left[1-\frac{\tanh(kh)}{kh}\right] - U\frac{2k^2}{h^2 b}\sum_{n=0}^{\infty}\frac{\tanh(\beta_n b)}{\alpha_n^2\beta_n^3}, \end{aligned} \tag{10}$$

where m in suffix denotes averaging over the cross-section. Note that $u_m \to U$ as $kh \to \infty$.

A neutral species of dilute concentration C is to be carried with the fluid. The species is neutral so that the transport phenomenon will not be affected by any of the electrical potentials. The convection–diffusion equation governing the concentration $C(t,x,y,z)$ can be written as

$$\frac{\partial C}{\partial t} + u(x,y)\frac{\partial C}{\partial z} = D\left(\frac{\partial^2 C}{\partial x^2} + \frac{\partial^2 C}{\partial y^2} + \frac{\partial^2 C}{\partial z^2}\right), \tag{11}$$

where D is the molecular diffusion coefficient.

Equation (11) is subject to the following initial and boundary conditions:

$$C(0,x,y,z) = \delta(z)\phi(x,y), \tag{12}$$

$$\frac{\partial C}{\partial x} = 0 \quad \text{at} \quad x = \pm b, \tag{13}$$

$$\frac{\partial C}{\partial y} = 0 \quad \text{at} \quad y = \pm h. \tag{14}$$

Here $\delta(z)$ is the Dirac delta function and $\phi(x,y)$ specifies the source strength and location. It represents an initial distribution highly concentrated (i.e., a narrow slug) at the origin $z = 0$. We remark that the initial concentration distribution will have effects only on the early time development of the transport coefficients, but not on their steady-state limits. Equations (13)–(14) mean that there is no material transport across the walls of the channel. Due to symmetry, the gradients at $x = 0$ and at $y = 0$ must be zero, i.e.,

$$\frac{\partial C}{\partial x} = 0 \quad \text{at} \quad x = 0, \tag{15}$$

$$\frac{\partial C}{\partial y} = 0 \quad \text{at} \quad y = 0. \tag{16}$$

The fact that the species never reaches points very far from the source at a finite time can be represented mathematically by

$$C(t,x,y,\infty) = \frac{\partial C}{\partial z}(t,x,y,\infty) = 0. \tag{17}$$

If the side walls are to be neglected, the equations deduced above will be simplified considerably since then the dependence on x will disappear: there will be no diffusion in the x-direction, and the velocity profile becomes a function of y only. This case of flow and transport through a parallel-plate channel will be considered later in Sec. 3.

2.2 Generalized dispersion theory

The general procedure of Gill and Sankarasubramanian [13] is followed here to evaluate the dispersion coefficient for all times. Following the approach of Doshi et al. [1], the concentration C can be expanded as a function of four independent variables as

$$C(t,x,y,z) = \sum_{n=0}^{\infty} f_n(t,x,y) \frac{\partial^n C_m}{\partial z^n}, \tag{18}$$

where the mean concentration C_m is defined as

$$C_m(t,z) = \frac{1}{4bh} \int_{-h}^{h} \int_{-b}^{b} C dx dy. \tag{19}$$

From Eqs. (18) and (19) we have

$$\frac{1}{4bh} \int_{-h}^{h} \int_{-b}^{b} f_n dx dy = \delta_{n0}. \tag{20}$$

Integration of Eq. (11) over the cross section gives

$$\frac{\partial C_m}{\partial t} = D \frac{\partial^2 C_m}{\partial z^2} - \frac{1}{4bh} \frac{\partial}{\partial z} \left(\int_{-h}^{h} \int_{-b}^{b} u C dx dy \right). \tag{21}$$

Now substituting the local concentration from Eq. (18) into Eq. (21) and rearranging, we have the generalized dispersion equation for $C_m(t,z)$ as

$$\frac{\partial C_m}{\partial t} = \sum_{n=1}^{\infty} K_n(t) \frac{\partial^n C_m}{\partial z^n}, \tag{22}$$

where the coefficients $K_n(t)$ are given by

$$K_n(t) = -\frac{1}{4bh} \int_{-h}^{h} \int_{-b}^{b} u f_{n-1} dx dy + \delta_{n2} D, \tag{23}$$

in which δ_{n2} is the Kronecker delta (i.e., $\delta_{n2} = 1$ for $n = 2$ and $\delta_{n2} = 0$ for $n \neq 2$).

The coefficients of the first two terms of the expansion (22), $-K_1$ and K_2, are termed respectively the convection and dispersion coefficients. The third and the fourth coefficients, K_3 and K_4, provide information about the skewness and kurtosis (roundness) of the concentration distribution. They serve as simple and physically meaningful descriptors of the overall transport behaviors of the solute in the stream. In this study, we shall focus only on the first two coefficients. The convection coefficient determines the rate of movement of the center of the solute cloud distribution, while the dispersion coefficient controls the rate of broadening of the distribution about its center. More precisely, the dispersion coefficient is equal to half the rate of increase of the variance of the distribution.

Equation (22) may be solved for $C_m(t,z)$ if the coefficients $K_n(t)$ are known. This requires a knowledge of the functions $f_n(t,x,y)$. To find these, Eq. (18) representing the solution will be substituted into Eq. (11). After evaluating the mixed derivatives of the form $\partial^{k+1}C_m/\partial t\partial z^k$ in terms of $\partial^i C_m/\partial z^i$ by suitable differentiation of Eq. (22), and setting the coefficients of $\partial^k C_m/\partial z^k$ to zero for each k, the following set of defining differential equations for the functions f_n may be obtained:

$$\frac{\partial f_n}{\partial t} + (u + K_1) f_{n-1} = D\left(\frac{\partial^2 f_n}{\partial x^2} + \frac{\partial^2 f_n}{\partial y^2}\right) + (D - K_2) f_{n-2} - \sum_{i=3}^{n} f_{n-i} K_i, \tag{24}$$

with $f_{-1} = f_{-2} = 0$.

The corresponding boundary conditions can be obtained from Eqs. (13)–(16) as

$$\left.\frac{\partial f_n}{\partial x}\right|_{x=0,\,\pm b} = 0, \tag{25}$$

$$\left.\frac{\partial f_n}{\partial y}\right|_{y=0,\,\pm h} = 0. \tag{26}$$

To find the initial condition for f_n, we have from Eqs. (12) and (18),

$$C(0,x,y,z) = \sum_{n=0}^{\infty} f_n(0,x,y)\frac{\partial^n C_m}{\partial z^n}(0,z) = \delta(z)\phi(x,y),$$

which gives

$$f_n(0,x,y) = \begin{cases} \phi(x,y)/\phi_m & \text{if} \quad n = 0 \\ 0 & \text{if} \quad n \neq 0 \end{cases}, \tag{27}$$

where

$$\phi_m = \frac{1}{4bh}\int_{-h}^{h}\int_{-b}^{b}\phi(x,y)dxdy \tag{28}$$

is the cross-sectional average of $\phi(x,y)$.

If the solute is initially distributed occupying only part of the cross section, in a rectangular region of height $2h_s$ and width $2b_s$ that is symmetrical about the x- and y-axes (see Fig. 1), then $\phi(x,y)$ can be expressed as

$$\phi(x,y) = \begin{cases} C_0 & \text{if } -h_s \le y \le h_s \text{ and } -b_s \le x \le b_s \\ 0 & \text{otherwise} \end{cases}, \tag{29}$$

where C_0 is a constant.

2.3 Determination of transport coefficients

The equation determining the function f_0 can be written from Eq. (24) as

$$\frac{\partial f_0}{\partial t} = D\left(\frac{\partial^2 f_0}{\partial x^2} + \frac{\partial^2 f_0}{\partial y^2}\right). \tag{30}$$

From Eqs. (28), (27) and (29), the initial condition for f_0 can be written as

$$f_0(0,x,y) = \begin{cases} bh/b_s h_s & \text{if } -h_s \le y \le h_s \text{ and } -b_s \le x \le b_s \\ 0 & \text{otherwise} \end{cases}. \tag{31}$$

Using the method of separation of variables, the solution of Eq. (30) subject to the boundary conditions (25) and (26) can be written as

$$f_0(t,x,y) = \sum_{m=0}^{\infty}\sum_{n=0}^{\infty} A_{mn}\cos(\gamma_m x)\cos(\eta_n y)\exp\left[-tD\left(\gamma_m^2+\eta_n^2\right)\right], \tag{32}$$

where

$$\gamma_m = m\pi/b, \qquad \eta_n = n\pi/h. \tag{33}$$

The integrability condition (20) gives

$$A_{00} = 1, \tag{34}$$

while the initial condition (31) gives

$$A_{m0} = \frac{2}{\gamma_m b_s}\sin(\gamma_m b_s), \tag{35}$$

$$A_{0n} = \frac{2}{\eta_n h_s}\sin(\eta_n h_s), \tag{36}$$

$$A_{mn} = \frac{4}{\gamma_m \eta_n b_s h_s}\sin(\gamma_m b_s)\sin(\eta_n h_s). \tag{37}$$

With f_0 from (32) and u from (9), the convection coefficient $-K_1$ can now be derived from Eq. (23) as

$$\begin{aligned} -K_1(t) &= U\left[1-\frac{\tanh(kh)}{kh}\right] - U\sum_{n=1}^{\infty} A_{0n}\frac{(-1)^n kh\tanh(kh)}{k^2h^2+n^2\pi^2}\exp\left(-tD\eta_n^2\right) \\ &\quad - U\frac{2k^2}{h^2}\sum_{j=0}^{\infty}\frac{\tanh(\beta_j b)}{\beta_j b}\sum_{m=0}^{\infty}\sum_{n=0}^{\infty}\frac{(-1)^{m+n}A_{mn}\exp\left[-tD\left(\gamma_m^2+\eta_n^2\right)\right]}{(\alpha_j^2-\eta_n^2)(\beta_j^2+\gamma_m^2)}. \end{aligned} \tag{38}$$

Some analytical properties of the convection coefficient can be deduced as follows. First, the large-time limit of this coefficient, i.e., its steady-state value, is equal to the section-average fluid velocity u_m, which has been given in Eq. (10):

$$\lim_{t\to\infty} -K_1(t) = u_m = U\left[1-\frac{\tanh(kh)}{kh}\right] - U\frac{2k^2}{h^2 b}\sum_{n=0}^{\infty}\frac{\tanh(\beta_n b)}{\alpha_n^2\beta_n^3}. \tag{39}$$

Second, the limiting value of the coefficient in the case of very large aspect ratio (i.e., $\lambda \gg 1$) is given by

$$\lim_{\lambda\gg 1} -K_1(t) = U\left[1-\frac{\tanh(kh)}{kh}\right] - U\sum_{n=1}^{\infty} A_{0n}\frac{(-1)^n kh\tanh(kh)}{k^2h^2+n^2\pi^2}\exp\left(-tD\eta_n^2\right), \tag{40}$$

which, as will be seen later, is equal to that for flow in a parallel-plate channel. Third, when the initial distribution occupies the entire cross section so that $h_s = h$ and $b_s = b$, then there follows a considerable simplification of the problem and it is easy to see from Eqs. (32)–(37) that $f_0 = 1$. With this simplified f_0, the convection coefficient becomes independent of time, and is equal to the section-average fluid velocity at all times: $-K_1 = u_m$.

From Eq. (24), the equation governing f_1 is

$$\frac{\partial f_1}{\partial t} = D\left(\frac{\partial^2 f_1}{\partial x^2}+\frac{\partial^2 f_1}{\partial y^2}\right) - (u+K_1)f_0. \tag{41}$$

Solving this non-homogeneous equation is tedious because of the intricate form of f_0 and K_1 in Eqs. (32) and (38) respectively. To avoid the mathematical complexity, we shall from

here on assume an initial distribution of solute uniformly occupying the entire cross section. Under this condition, as already given above, $f_0 = 1$ and $-K_1 = u_m$ are much simpler in form and independent of time, which will greatly simplify our efforts in computing the dispersion coefficient.

With this assumption, the solution of Eq. (41) subject to the initial condition (27) and boundary conditions (25) and (26) is

$$f_1 = \sum_{m=0}^{\infty}\sum_{n=0}^{\infty} B_{mn}\cos(\eta_n y)\cos(\gamma_m x)\left\{1-\exp\left[-tD\left(\gamma_m^2+\eta_n^2\right)\right]\right\}. \tag{42}$$

where

$$B_{00} = 0, \tag{43}$$

$$B_{m0} = \frac{4}{\pi^2}\frac{Uk^2b}{Dh^2}\frac{(-1)^m}{m^2}S_{m0}, \tag{44}$$

$$B_{0n} = 2\frac{Uh^2}{D}\frac{(-1)^n kh\tanh(kh)}{n^2\pi^2(k^2h^2+n^2\pi^2)} + \frac{4}{\pi^2}\frac{Uk^2}{Db}\frac{(-1)^n}{n^2}S_{0n}, \tag{45}$$

$$B_{mn} = \frac{8}{\pi^2}\frac{Uk^2b}{D}\frac{(-1)^{m+n}}{m^2h^2+n^2b^2}S_{mn}, \tag{46}$$

in which

$$S_{m0} = \sum_{j=0}^{\infty}\frac{\tanh(\beta_j b)}{\alpha_j^2\beta_j\left(\beta_j^2+\gamma_m^2\right)}, \tag{47}$$

$$S_{0n} = \sum_{j=0}^{\infty}\frac{\tanh(\beta_j b)}{\beta_j^3\left(\alpha_j^2-\eta_n^2\right)}, \tag{48}$$

$$S_{mn} = \sum_{j=0}^{\infty}\frac{\tanh(\beta_j b)}{\beta_j\left(\alpha_j^2-\eta_n^2\right)\left(\beta_j^2+\gamma_m^2\right)}. \tag{49}$$

With this f_1, the dispersion coefficient K_2 can be obtained from Eq. (23) as

$$\begin{aligned} K_2(t) &= D + D\left(\frac{Uh}{D}\right)^2\left\{\frac{8}{\pi^2}\frac{k^4}{h^6}\sum_{m=1}^{\infty}\frac{S_{m0}^2}{m^2}\left[1-\exp\left(-tD\gamma_m^2\right)\right]\right. \\ &\quad + \frac{2}{\pi^2}\sum_{n=1}^{\infty}\left(\frac{kh\tanh(kh)}{n(k^2h^2+n^2\pi^2)} + 2\frac{k^2}{h^2b}\frac{S_{0n}}{n}\right)^2\left[1-\exp\left(-tD\eta_n^2\right)\right] \\ &\quad \left. + \frac{16}{\pi^2}\frac{k^4}{h^4}\sum_{m=1}^{\infty}\sum_{n=1}^{\infty}\frac{S_{mn}^2}{m^2h^2+n^2b^2}\left(1-\exp\left[-tD\left(\gamma_m^2+\eta_n^2\right)\right]\right)\right\}. \end{aligned} \tag{50}$$

This is the general formula for the dispersion coefficient in the present study. Because of the squared terms in the series, the dispersion coefficient is obviously positive definite, at all

times and for any parameter values. In the limit of very large aspect ratio, the expression above for the dispersion coefficient reduces to

$$\lim_{\lambda\gg 1} K_2(t) = D + D\left(\frac{Uh}{D}\right)^2 \left\{ \frac{8}{\pi^2}\frac{k^4}{h^6}\left(\sum_{j=0}^{\infty}\frac{1}{\alpha_j^2\beta_j^3}\right)^2 \sum_{m=1}^{\infty}\frac{[1-\exp(-tD\gamma_m^2)]}{m^2} + \frac{2}{\pi^2}k^2h^2\tanh^2(kh)\sum_{n=1}^{\infty}\frac{[1-\exp(-tD\eta_n^2)]}{n^2(k^2h^2+n^2\pi^2)^2}\right\}. \quad (51)$$

Doshi et al. [1] showed that the dispersion coefficients obtained by adding the two dispersion coefficients, each neglecting the gradients of velocity and concentration in one direction, can be a very good approximation to the estimation of the actual dispersion coefficient, particularly in the limit of very large aspect ratio. To examine its validity with regard to the present analysis, let us consider two special cases by ignoring the velocity/concentration gradients in the vertical (y) and the horizontal (x) directions.

When vertical gradients ignored

To obtain the dispersion coefficient by neglecting the vertical gradients of the concentration and velocity in Eq. (11), we consider the depth-averaged velocity profile and accordingly modify Eq. (11) to give:

$$\frac{\partial C_1}{\partial t} + \left(\frac{1}{2h}\int_{-h}^{h} u dy\right)\frac{\partial C_1}{\partial z} = D\left(\frac{\partial^2 C_1}{\partial x^2} + \frac{\partial^2 C_1}{\partial z^2}\right). \quad (52)$$

By following the procedure already explained, the dispersion coefficient based on the horizontal velocity gradient only can be readily found as

$$[K_2(t)]_{\substack{\text{based on horizontal}\\ \text{gradient only}}} = D + D\left(\frac{Uh}{D}\right)^2 \frac{8}{\pi^2}\frac{k^4}{h^6}\sum_{m=1}^{\infty}\frac{S_{m0}^2}{m^2}\left[1-\exp\left(-tD\gamma_m^2\right)\right], \quad (53)$$

where S_{m0} is given in Eq. (47).

When horizontal gradients ignored

Analogously, on neglecting the horizontal gradients of velocity and concentration, one obtains

$$[K_2(t)]_{\substack{\text{based on vertical}\\ \text{gradients only}}} = D + D\left(\frac{Uh}{D}\right)^2 \frac{2}{\pi^2}\sum_{n=1}^{\infty}\left(\frac{kh\tanh(kh)}{n(k^2h^2+n^2\pi^2)} + 2\frac{k^2}{h^2 b}\frac{S_{0n}}{n}\right)^2 \times\left[1-\exp\left(-tD\eta_n^2\right)\right], \quad (54)$$

where S_{0n} is given in Eq. (48).

It is interesting to note that Eqs. (53) and (54) are terms in Eq. (50); these approximate expressions are components in the full expression of the dispersion coefficient.

2.4 Approximate dispersion coefficient

From Eqs. (51), (53) and (54), one can readily see that the effect of vertical and horizontal gradients is indeed additive as the aspect ratio becomes very large. This observation has led Doshi et al. [1] to suggest a very simple way to approximate the dispersion coefficient when side wall effects are present. The contributions made by horizontal gradients only, Eq. (53), and by vertical gradients only, Eq. (54), can be simply combined by addition to give an approximate dispersion coefficient:

$$\begin{aligned}[K_2(t)]_{\text{approx}} &= D + D\left(\frac{Uh}{D}\right)^2 \left\{ \frac{8}{\pi^2}\frac{k^4}{h^6}\sum_{m=1}^{\infty}\frac{S_{m0}^2}{m^2}\left[1-\exp\left(-tD\gamma_m^2\right)\right] \right. \\ &\left. + \frac{2}{\pi^2}\sum_{n=1}^{\infty}\left(\frac{kh\tanh(kh)}{n(k^2h^2+n^2\pi^2)} + 2\frac{k^2}{h^2 b}\frac{S_{0n}}{n}\right)^2\left[1-\exp\left(-tD\eta_n^2\right)\right]\right\} \quad (55)\end{aligned}$$

The error in Eq. (55) is equal to the last term on the right-hand side of Eq. (50), which diminishes with the increase of the aspect ratio, $\lambda = b/h$, or $\lim_{\lambda\gg 1} K_2(t) = [K_2(t)]_{\text{approx}}$, a better approximation given by Eq. (55) for a larger aspect ratio.

The analytical expressions for the time-dependent transport coefficients for an electroosmotic flow through a rectangular microchannel are now deduced. As our main concern is to look into the effect of side walls of the microchannel on the transport coefficients, let us now proceed to find the same for flow through a parallel-plate channel so that the side wall effects can be determined through comparison of the two cases.

3 Flow and transport in a parallel-plate channel

In this section, we consider electroosmotic flow through a two-dimensional microchannel of height $2h$ formed by two parallel plates as shown in Fig. 1(b). The z-axis is along the flow, and the y-axis is normal to the flow. The boundaries are at $y = \pm h$.

For the present planar steady flow caused solely by electroosmotic mechanism, the fluid velocity is given by

$$u_{\parallel}(y) = U\left[1 - \frac{\cosh(ky)}{\cosh(kh)}\right], \tag{56}$$

where $U = -\epsilon E\zeta/\mu$ is the Helmholtz–Smoluchowski velocity, E is the applied electric field in the axial direction, ζ is the zeta potential at the walls $y = \pm h$, and k is the reciprocal of the Debye length. The velocity averaged over the cross section of the channel is

$$u_{m\parallel} = \frac{1}{2h}\int_{-h}^{h} u_{\parallel}(y)dy = U\left[1 - \frac{\tanh(kh)}{kh}\right]. \tag{57}$$

Following analogous steps already explained in the previous section, the convection coefficient for the parallel-plate configuration in the case of an initial distribution of solute of depth $2h_s$ can be written as

$$-K_{1\parallel}(t) = U\left[1 - \frac{\tanh(kh)}{kh}\right] - U\sum_{n=1}^{\infty}\frac{2(-1)^n \sin(\eta_n h_s)}{\eta_n h_s}\frac{kh\tanh(kh)}{k^2h^2 + n^2\pi^2}\exp\left(-tD\eta_n^2\right), \tag{58}$$

which is equal to $\lim_{\lambda\gg 1} -K_1(t)$ given in Eq. (40). Also, at large times, $\lim_{t\to\infty} -K_{1\parallel} = u_{m\parallel}$.

From Eqs. (40) and (58), it can be remarked that the convection coefficient for transport in a rectangular microchannel will reduce to that in a parallel-plate channel (without the side walls effects) in the limit of very large aspect ratio, as was found by Doshi et al. [1].

In the case of an initial distribution of solute occupying the entire section (i.e., $h_s = h$), the convection coefficient $K_{1\parallel}$ is steady, equal to the section-average fluid velocity, at all times: $-K_{1\parallel} = u_{m\parallel}$. With this steady $K_{1\parallel}$, the dispersion coefficient $K_{2\parallel}(t)$ for the parallel-plate geometry can be written as

$$K_{2\parallel}(t) = D + D\left(\frac{Uh}{D}\right)^2\frac{2}{\pi^2}\sum_{n=1}^{\infty}\frac{k^2h^2\tanh^2(kh)}{n^2(k^2h^2 + n^2\pi^2)^2}\left[1 - \exp\left(-tD\eta_n^2\right)\right]. \tag{59}$$

This expression contains all except one series of terms in the expression (51) obtained for transport in a rectangular microchannel in the limit of very large aspect ratio. Hence, the dispersion coefficient for a rectangular channel of very large aspect ratio does not exactly reduce to that for a parallel-plate channel. The series of terms missing here are multiplied by the factor $[1 - \exp(-tD\gamma_m^2)]$, which is identically zero only when $tD\gamma_m^2 = 0$ or when the channel width is absolutely infinite $b = \infty$ for finite time t. For a very large but finite aspect

ratio $1 \ll \lambda < \infty$, the long-time asymptotic dispersion coefficient for a rectangular channel is in general different from the dispersion coefficient for a parallel-plate channel. We note in passing that Eq. (59) has a closed-form expression for the steady state:

$$\lim_{t\to\infty} K_{2\|} = D + D\left(\frac{Uh}{D}\right)^2 \left[\frac{2\tanh^2(kh)}{(kh)^4} + \frac{5\tanh^2(kh)}{6(kh)^2} - \frac{3\tanh(kh)}{2(kh)^3} - \frac{1}{2(kh)^2}\right], \tag{60}$$

which agrees with the one deduced by Griffiths and Nilson [16].

4 To check with the theory of Desmet and Baron [12]

Flow and transport coefficients associated with rectangular and parallel-plate channels have been derived in Secs. 2 and 3, respectively. It was shown by Desmet and Baron [12] that the additional dispersion effect due to the side walls in a rectangular channel in the steady state can be quantified by assuming the presence of a pseudo-stationary layer near the side walls. The thickness of this layer d can be evaluated from the retardation of the fluid flow by the channel side walls as

$$\frac{d}{h} = \lim_{\lambda\gg 1} \frac{b}{h}\left(1 - \frac{u_m}{u_{m\|}}\right) = \frac{2k^3}{h^2[kh - \tanh(kh)]} \sum_{n=0}^{\infty} \frac{1}{\alpha_n^2 \beta_n^3}, \tag{61}$$

where Eqs. (10) and (57) have been used for u_m and $u_{m\|}$. According to Desmet and Baron [12], the thickness of the pseudo-stationary layer given by Eq. (61) may then be used to evaluate the additional dispersivity in a rectangular channel due to the side walls as

$$K_2^W = \frac{D}{3}\left(\frac{u_{m\|}h}{D}\right)^2 \left(\frac{d}{h}\right)^2 = D\left(\frac{Uh}{D}\right)^2 \frac{4k^4}{3h^6} \left(\sum_{n=0}^{\infty} \frac{1}{\alpha_n^2 \beta_n^3}\right)^2. \tag{62}$$

As the contribution to dispersion from fluid shear across the vertical and horizontal directions of a large-aspect-ratio channel are additive [1], the steady-state (i.e., when $t \to \infty$) dispersion coefficient in the limit $\lambda \gg 1$ can be expressed as:

$$\lim_{\substack{\lambda\gg 1 \\ t\to\infty}} K_2 = \lim_{t\to\infty} K_{2\|} + K_2^W. \tag{63}$$

From Eqs. (51) and (59), by which one easily gets the steady-state limits of $\lim_{\lambda\gg 1} K_2$ and $K_{2\|}$, and using Eq. (62) for K_2^W, one can check that Eq. (63) is indeed satisfied. This shows the exact agreement of the present model with the theory of Desmet and Baron [12].

5 Discussion of results

Let us now proceed to look into the time development of the side wall effects of a rectangular microchannel on the transport coefficients from their analytical expressions. As it is more convenient to show results in dimensionless form, we have used the following dimensionless quantities (distinguished by a caret) for the computations:

$$\lambda = \frac{b}{h}, \quad \hat{k} = kh, \quad \hat{t} = \frac{tD}{h^2}, \quad Pe = \frac{Uh}{D}, \quad \hat{K_1} = \frac{K_1}{U}, \quad \hat{K_2} = \frac{K_2}{D}. \tag{64}$$

Here λ is the aspect ratio of the channel, and Pe is the Péclet number that measures the relative characteristic time of the diffusion process across half the channel height ($T_0 = h^2/D$) to the convection process over an axial distance equal to half the channel height ($T_c = h/U$). The time variable t has been non-dimensionalized with respect to T_0, the time scale for diffusion across half the channel height h. All length scales have been normalized in this problem by the half height h of the rectangular or parallel-plate channel. Unlike Dutta [8, 9], who used the section-average velocity u_m as the velocity scale for the normalization (and in the definition of the Péclet number), we have chosen the Helmholtz–Smoluchowski velocity U as the velocity scale instead. The reason for our choice is that U does not depend on the Debye–Hückel parameter $\hat{k}$, while u_m varies with $\hat{k}$. Our choice will enable us to examine the proper dependence of the results on the parameter $\hat{k}$.

As stated in the introduction, the main objective of this paper is to investigate the temporal variations of the side wall effects on the electroosmotic transport of a neutral solute in a rectangular channel. Following the approach of Doshi et al. [1], the transport coefficients have been obtained using the generalized dispersion model. In order to compute these coefficients, we need to specify the aspect ratio λ of the channel, and the dimensionless Debye–Hückel parameter $\hat{k}$ representing the ratio of half the channel height to the EDL thickness. In general, microchannels are fabricated to have a very large aspect ratio [17] compared with ordinary rectangular channels. The range of the aspect ratio to be considered for the present analysis is taken as $1 \leq \lambda \leq 10^3$. For numerical discussions, the range of the dimensionless Debye–Hückel parameter is taken as $1 < \hat{k} \leq 100$. These values are frequently reported in the literature [18, 19, 20] for typical scenarios of electroosmotic flow.

Figure 2(a) shows the dimensionless convection coefficient $-\hat{K_1} = u_m/U$, given in Eq.

(10), as a function of the aspect ratio λ for different values of the Debye–Hückel parameter $\hat{k}$. The values corresponding to the parallel-plate geometry are also shown in the figure for comparison. The convection coefficient increases monotonically with the aspect ratio λ for constant $\hat{k}$. When λ exceeds 100, the convection coefficient for the rectangular microchannel is practically the same as the value for the parallel-plate configuration. Thus the convection coefficient for flow through a rectangular microchannel can be approximated by that through a parallel-plate geometry only when the aspect ratio of the channel is of order 100 or larger. The convection coefficient is shown as a function of the Debye–Hückel parameter $\hat{k}$ in Fig. 2(b) for different values of the aspect ratio λ. The monotonic increase of the convection coefficient with $\hat{k}$, for any aspect ratio, is evident from the figure. As $\hat{k} \to \infty$, $-\hat{K}_1 \to 1$ for any λ. Hence, irrespective of the aspect ratio, the convection coefficient will be equal to the Helmholtz–Smoluchowski velocity, which is the plug-flow electroosmotic velocity, in the limit of a very thin EDL.

The quantity $(\hat{K}_2 - 1)/Pe^2$, which is the numerical factor of the dispersion coefficient, given by the terms inside the parentheses in Eq. (50), is plotted in Fig. 3(a) as a function of the dimensionless time $\hat{t} = tD/h^2$ for different values of the aspect ratio λ and the Debye–Hückel parameter $\hat{k}$. At small times, for any large but finite aspect ratio, the dispersion coefficient is practically the same as that of the corresponding parallel-plate channel, implying that the side walls are yet to have significant effect at this early stage. As time increases, the dispersion coefficient will gradually branch out from that of the parallel-plate channel, where the branching out happens earlier for a smaller aspect ratio. After branching out, the coefficient will continue to increase with time until it ultimately reaches an asymptotic steady value at large times. This large-time asymptotic value, under the side wall effects, can be several times larger than the counterpart without the side walls.

There are several time scales that are of interest in the time development of the dispersion processes shown in Fig. 3. First, recall that the basic time scale T_0, by which the time variable t is normalized, corresponds to the time scale for molecular diffusion, which is responsible for smoothing out any concentration variations, across the channel height. For $t \leq O(T_0)$, the time is too short for the side walls to have significant effect on the transport. Therefore, during this very early stage, the dispersion evolves with time as if it were in a parallel-plate

channel. At small times, when the transport is convection-dominated, the section-mean concentration distribution is highly skewed and non-Gaussian. As diffusion takes effect in bringing solute near the walls into the faster moving parts of the fluid near the center of the channel and vice versa, the distribution will be increasingly symmetrical, approaching a Gaussian distribution in the long run when the interaction between lateral diffusion and axial convection reaches an equilibrium state. By this stage, the transience dies out and the dispersion is fully developed; all the transport coefficients become independent of time when fully developed. Ng and Rudraiah [21] and Ng [22] can be consulted for further descriptions about early-time development of the transport processes.

Therefore, the earliest (also the shortest) transience for the development of the dispersion in a rectangular channel of large aspect ratio is the same as that in a parallel-plate channel. The transience is of a time scale comparable to T_0, and from Eq. (59), the slowest exponential decay happens over the dimensionless time scale $1/\pi^2$. From our results, such as those shown in Fig. 3(b), which is a magnified view of the profiles for $\hat{k} = 100$, we may infer that the transient time is approximately four times this time scale. The dispersion coefficient is fully developed for a parallel-plate channel over a short time given by $T_1 = 4/\pi^2 \sim 0.4$.

After the first transience dies out, the second transience comes in, and is controlled by diffusion across the channel breadth, which takes a much longer time depending on the aspect ratio. For a sufficiently large aspect ratio, there is an interlude of steadiness between the two transient periods. It is temporarily steady because the time is long enough for the first transience (associated with diffusion across the channel height) to vanish, but still too early for the second transience (arising from diffusion across the channel breadth) to gain effect. Within this time interval the dispersion coefficient is as steady as that of the parallel-plate channel. This is the period in which K_2 is nearly equal to $K_{2\|}$, which can be materialized when $1 - \exp(-tD\gamma_m^2) \approx 0$. We can infer from our results shown in Fig. 3 that this time interval is approximately given by $\hat{t} < T_2 = 10^{-3}(\lambda/\pi)^2$. This time scale is of relevance only when $T_2 > T_1$, or $\lambda > 63$. For smaller λ, this interlude does not exist. The larger the aspect ratio is, the longer this temporary period of steadiness will last.

Upon deviating from the parallel-plate value, the dispersion coefficient for a rectangular channel will further evolve with time at a rate controlled by γ_m^2, which is inversely propor-

tional to the square of the channel breadth b. The time required to attain the large-time limit is a function of the aspect ratio. The larger the aspect ratio, the longer the time required for this second transient development. From Eq. (50), one can check that the slowest varying term, which is the one with the lowest γ_m, is scaled by the dimensionless time $(\lambda/\pi)^2$. From the magnified view shown in Fig. 3(b), we can again infer that the second transient time T_3 is approximately four times this time scale: $T_3 \sim 4(\lambda/\pi)^2$. As in the first transient period, the mean concentration distribution will be skewed and non-Gaussian during the second transient period.

In summary, the dispersion coefficient for a rectangular channel of sufficiently large aspect ratio will undergo several stages of development with time. First, $\hat{t} < T_1$, first transience as if it were a parallel-plate channel. Second, $T_1 < \hat{t} < T_2$, nearly steady as if it were a parallel-plate channel. Third, $T_2 < \hat{t} < T_3$, second transience under the side wall effects. Fourth, $\hat{t} > T_3$, steady and fully developed. For a very large aspect ratio, say $\lambda = 500$, the time required for the dispersion coefficient to be fully developed is of the order 10^5, which may far exceed the time scale for the operation of processes taking place in a microchannel. One has to be mindful of these time scales on deciding which value of the dispersion coefficient is appropriate to use for a particular application.

Figure 3(b) also shows that, for the parallel-plate configuration, the asymptotic steady value of the dispersion coefficient is 3.185×10^{-5}, whereas for a rectangular channel of large aspect ration, it is 6.39×10^{-5}. In fact, the steady dispersion coefficient of a rectangular channel is exactly twice that of the corresponding parallel-plate channel in the limit $\hat{k} \to \infty$. This result has been obtained previously by Zholkovskij et al. [3] and Dutta [8, 9].

The relative dispersion effect characterized by the ratio of the numerical factors of the dispersion coefficients for the two geometries, $(\hat{K}_2 - 1)/(\hat{K}_{2\|} - 1)$, is shown in Fig. 4(a, b, c), as a function of the aspect ratio λ at different instants of time. The same is presented in Fig. 4(d, e, f) as a function of the dimensionless Debye–Hückel parameter $\hat{k}$. It can be seen from Fig. 4(a) that at an early instant of time the ratio $(\hat{K}_2 - 1)/(\hat{K}_{2\|} - 1)$ approaches unity as the aspect ratio λ is larger than 100. At small times, the dispersion coefficient for a rectangular microchannel of an aspect ratio larger than 100 is not different from that without the side walls. As time increases, there is a substantial change in this threshold

value of λ. Fig. 4(b) shows that for time $\hat{t} = 10$, it requires λ to be nearly 10^3 for the agreement of the dispersion coefficients $\hat{K}_2$ and $\hat{K}_{2\parallel}$, especially for small $\hat{k}$. The scenario changes more at the asymptotic steady stage, which can be seen from Fig. 4(c). At this stage, the agreement in dispersion coefficient of the two configurations is never possible even for a very large aspect ratio. It is clear from the figure that the quantity $(\hat{K}_2 - 1)/(\hat{K}_{2\parallel} - 1)$ increases monotonically with an increase in λ, where the rate of increase is larger for smaller $\hat{k}$. In the limit of $\hat{k} \ll 1$, the ratio $(\hat{K}_2 - 1)/(\hat{K}_{2\parallel} - 1)$ tends to the value 7.95 when $\lambda \to \infty$. This limiting value of 7.95 is the same as the one derived previously by Doshi et al. [1] for dispersion in pressure-driven flow through a rectangular channel. This is due to the fact that the velocity profile of electroosmotic flow becomes increasingly similar to that of pressure-driven flow as the EDL thickens, $\hat{k} \to 0$ [23]. For a thinner EDL, $\hat{k} > 1$, weaker response from the ratio $(\hat{K}_2 - 1)/(\hat{K}_{2\parallel} - 1)$ is obtained when λ changes its value from small to large. This demonstrates that as the EDL becomes very thin, the side wall effect on the dispersion also weakens. For $\hat{k} \geq 100$, the aspect ratio has virtually no effect on the dispersion coefficient, which is in agreement with the observation by Zholkovskij et al. [3] and Dutta [8]. In the limit $\hat{k} \to \infty$, the dispersion in a rectangular channel is exactly twice that in a parallel-plate channel, as has been noted earlier.

The steady value of the ratio $(\hat{K}_2 - 1)/(\hat{K}_{2\parallel} - 1)$ is greater than unity except when $\hat{k}$ and λ are both near unity. Side walls effects are reversed in this case meaning that the dispersivity in a rectangular channel is smaller than that in a parallel-plate channel when the EDL is relatively thick. For small aspect-ratio profiles ($\lambda \approx 1$), the characteristic length scales for diffusion along the vertical and horizontal directions of the rectangle are nearly the same. In this case, the dispersivity is smaller in a rectangular conduit than that between two parallel plates for small $\hat{k}$ because the fluid shear introduced by the side walls is diluted by the thickened EDLs. In other words, the decreasing effect due to a smaller section-average velocity will outweigh the increasing effect due to the presence of the side walls when λ and $\hat{k}$ are both order unity or smaller.

For the same results but from a different perspective, the ratio $(\hat{K}_2 - 1)/(\hat{K}_{2\parallel} - 1)$ is shown in Fig. 4(d, e, f) as a function of $\hat{k}$. Again, one can see how the dispersion coefficient varies dramatically with time depending on $\hat{k}$ and λ. The trends featured in these plots can

be reasoned with our arguments presented above. We caution again that for a very large aspect ratio, the small-time value of the dispersion coefficient can be much different from the large-time asymptotic steady value, but the time it takes to reach the asymptotic value can be too long for it to be of relevance in practice.

Let us compare Fig. 4(f) here with Fig. 4 of Dutta [8], where both figures show the asymptotic steady value of the ratio of the numerical factors of the dispersion coefficients as a function of $\hat{k}$ for some discrete values of the aspect ratio. One may find that, except for the limiting case $\lambda \to \infty$, our profiles here are different from those shown by Dutta [8]. This discrepancy arises from the fact that Dutta [8] used the section-mean velocity u_m in defining the Péclet number. One recalls that to get the dispersion coefficient, the numerical factor is to be multiplied by the square of the Péclet number. The mean velocity of flow in a rectangular channel, u_m, is in general different from that in a parallel-plate channel, $u_{m\|}$, both being functions of $\hat{k}$. Hence, in Dutta's formulation, the ratio of the numerical factors is not a full reflection of the ratio of the dispersion coefficients because the Péclet numbers do not cancel each other in the division. In our formulation, the Helmholtz–Smoluchowski velocity U, which is independent of the geometry and the parameter $\hat{k}$, is used in defining the Péclet number. Hence, our results shown in Fig. 4(f) can fully reveal the dependence of the ratio of the dispersion coefficients on $\hat{k}$. More precisely, our ratio of the numerical factors is equal to Dutta's ratio times $(u_m/u_{m\|})^2$.

6 Concluding remarks

Most of the existing studies on the effects of side walls on dispersion in a rectangular channel are restricted to the large-time asymptotic steady state. The time development of the side wall effects have not been addressed so far. In the present study, we have applied the generalized dispersion model to an investigation of the time evolution of the side wall effects on dispersion of an inert solute in electroosmotic flow through a rectangular microchannel. We have deduced analytical expressions for the convection and dispersion coefficients, as functions of time, the aspect ratio $\lambda = b/h$ and the Debye–Hückel parameter $\hat{k}$. The large-time limits are checked to be in agreement with those reported in the literature. We have shown

that the dispersion coefficient can vary dramatically with time following different trends depending on the aspect ratio and the Debye–Hückel parameter. A central question one would ask: can the dispersion coefficient for transport in a rectangular channel of very large aspect ratio be approximated by that in a parallel-plate channel? There is no single answer to this question: it depends on the time of the transport. We have identified several stages of time development. For $\hat{t} < T_1 = 4/\pi^2$, the dispersion coefficient changes with time as if it were a parallel-plate channel. This is followed by an interval $T_1 < \hat{t} < T_2 = 10^{-3}(\lambda/\pi)^2$, where the coefficient is nearly steady, again as if it were a parallel-plate channel. Up to this stage, the time is still too short for the side walls to have appreciable effects on the dispersivity. In the period $T_2 < \hat{t} < T_3 = 4(\lambda/\pi)^2$, the coefficient undergoes time development again, as the side walls gain their effects. Ultimately, when $\hat{t} > T_3$, the coefficient reaches its steady and fully-developed value. This asymptotic steady value is twice that for a parallel-plate channel for $\hat{k} \gg 1$ and any λ. The ratio of the steady dispersion coefficients for the two geometries can be as large as 7.95 for very small $\hat{k}$ and very large λ. We emphasize that one should take the time development of the dispersion process into account when deciding what value of the coefficient should be adopted in the analysis. For a channel of finite length, the residence time of solute in the channel may not be long enough for the fully-developed dispersion coefficient to be of relevance.

Acknowledgments

The work was supported by the Research Grants Council of the Hong Kong Special Administrative Region, China, through Project No. HKU 715510E, and by the University of Hong Kong through the Seed Funding Programme for Basic Research under Project Code 200911159024. Suvadip Paul is also grateful to the Directorate of Higher Education, Government of Tripura, India, for sanctioning leave for this work.

References

1. Doshi, M.R., Daiya, P.M., Gill, W.N.: Three dimensional laminar dispersion in open and closed rectangular conduits. Chem. Eng. Sci. **33**, 795–804 (1978)

2. Takahashi, T., Gill, W.N.: Hydrodynamic chromatography: three dimensional laminar dispersion in rectangular conduits with transverse flow. Chem. Eng. Commun. **5**, 367–385 (1980)

3. Zholkovskij, E.K., Masliyah, J.H., Czarnecki, J.: Electroosmotic dispersion in microchannels with a thin double layer. Anal. Chem. **75**, 901–909 (2003)

4. Dutta, D., Leighton, D.T.: Dispersion in large aspect ratio microchannels for open channel liquid chromatography. Anal. Chem. **75**, 57–70 (2003)

5. Zholkovskij, E.K., Masliyah, J.H.: Hydrodynamic dispersion due to combined pressure-driven and electroosmotic flow through microchannels with a thin double layer. Anal. Chem. **76**, 2708–2718 (2004)

6. A. Ajdari, N. Bontoux, H. A. Stone (2006) Hydrodynamic dispersion in shallow microchannels: the effect of cross sectional shape, Anal. Chem., 78, 387–392

7. Dutta, D., Ramachandran, A., Leighton, D.T.: Effect of channel geometry on solute dispersion in pressure-driven microfluidic systems. Microfluid. Nanofluid. **2**, 275–290 (2006)

8. Dutta, D.: Electroosmotic transport through rectangular channels with small zeta potentials. J. Colloid Interface Sci. **315**, 740–746 (2007)

9. Dutta, D.: Electrokinetic transport of charged samples through rectangular channels with small zeta potentials. Anal. Chem. **80**, 4723–4730 (2008)

10. Vikhansky, A.: Taylor dispersion in shallow micro-channels: aspect ratio effect. Microfluid. Nanofluid. **7**, 91–95 (2009)

11. Dutta, D.: Solutal transport in rectangular nanochannels under pressure-driven flow conditions. Microfluid. Nanofluid. **10**, 691–696 (2011)

12. Desmet, G., Baron, G.V.: Chromatographic explanation for the side-wall induced band broadening in pressure-driven and shear-driven flows through channels with a high aspect-ratio rectangular cross-section. J. Chromatogr. A **946**, 51–58 (2002)

13. Gill, W.N., Sankarasubramanian, R.: Exact analysis of unsteady convection diffusion. Proc. R. Soc. Lond. A **316**, 341–350 (1970)

14. Probstein, R.F.: Physicochemical Hydrodynamics. Wiley, New York (1994)

15. Li, D.Q.: Electrokinetics in Microfluidics. Elsevier, New York (2004)

16. Griffiths, S.K., Nilson, R.H.: Hydrodynamic dispersion of a neutral nonreacting solute in electroosmotic flow. Anal. Chem. **71**, 5522–5529 (1999)

17. Ren, L., Sinton, D., Li, D.: Numerical simulation of microfluidic injection processes in crossing microchannels. J. Micromech. Microeng. **13**, 739–747 (2003)

18. Kuo, C.Y., Wang, C.Y., Chang, C.C.: Generation of directional EOF by interactive oscillatory zeta potential. Electrophoresis **29**, 4386–4390 (2008)

19. Ramon, G., Agnon, Y., Dosoretz, C.: Solute dispersion in oscillating electro-osmotic flow with boundary mass exchange. Microfluid. Nanofluid. **10**, 97–106 (2011)

20. Paul, S., Ng, C.O.: Dispersion in electroosmotic flow generated by oscillatory electric field interacting with oscillatory wall potentials. Microfluid. Nanofluid. **12**, 237–256 (2012)

21. Ng, C.O., Rudraiah, N.: Convective diffusion in steady flow through a tube with a retentive and absorptive wall. Phys. Fluids **20**, 073604 (2008)

22. Ng, C.O.: How does wall slippage affect hydrodynamic dispersion? Microfluid. Nanofluid. **10**, 47–57 (2011)

23. Griffiths, S.K., Nilson, R.H.: Electroosmotic fluid motion and late-time solute transport for large zeta potentials. Anal. Chem. **72**, 4767–4777 (2000)

(a)

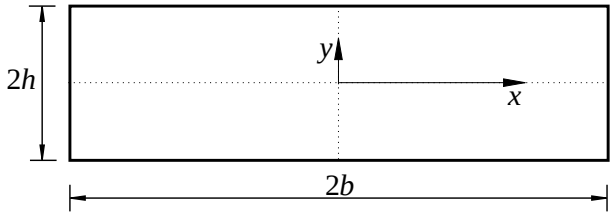

(b)

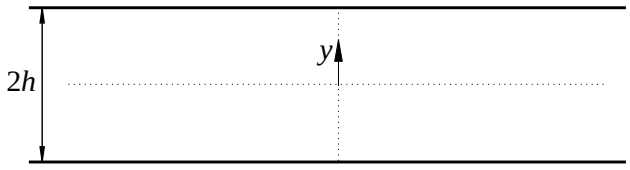

Figure 1: Cross section of a (a) rectangular microchannel of height $2h$ and breadth $2b$; (b) parallel-plate channel of height $2h$. The flow is along the z-axis perpendicular to the cross section.

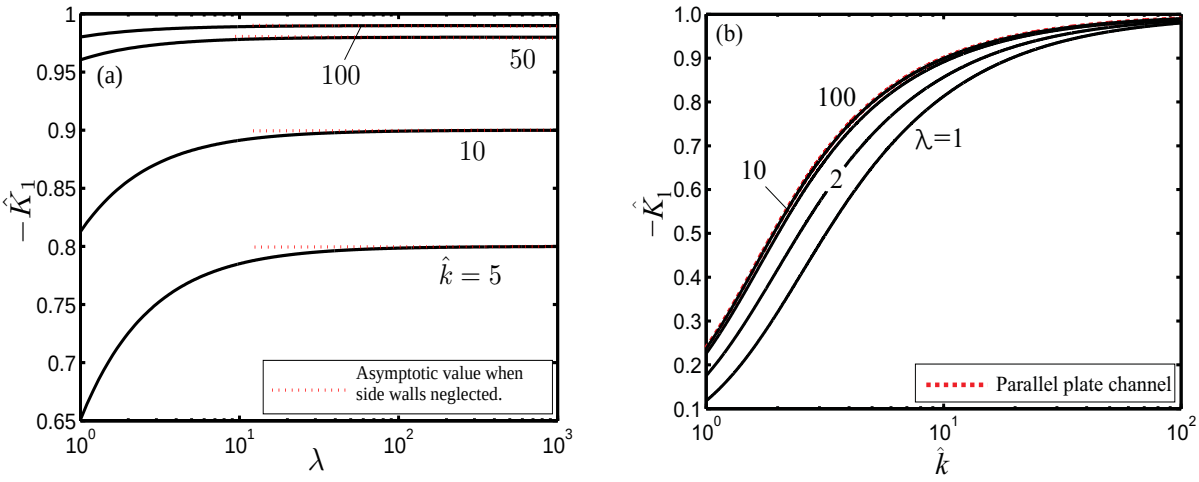

Figure 2: The convection coefficient, $-\hat{K}_1$, (a) as a function of the aspect ratio λ for different values of the Debye–Hückel parameter $\hat{k}$; (b) as a function of the Debye–Hückel parameter $\hat{k}$ for different values of the aspect ratio λ. The dotted lines are for the corresponding parallel-plate channel.

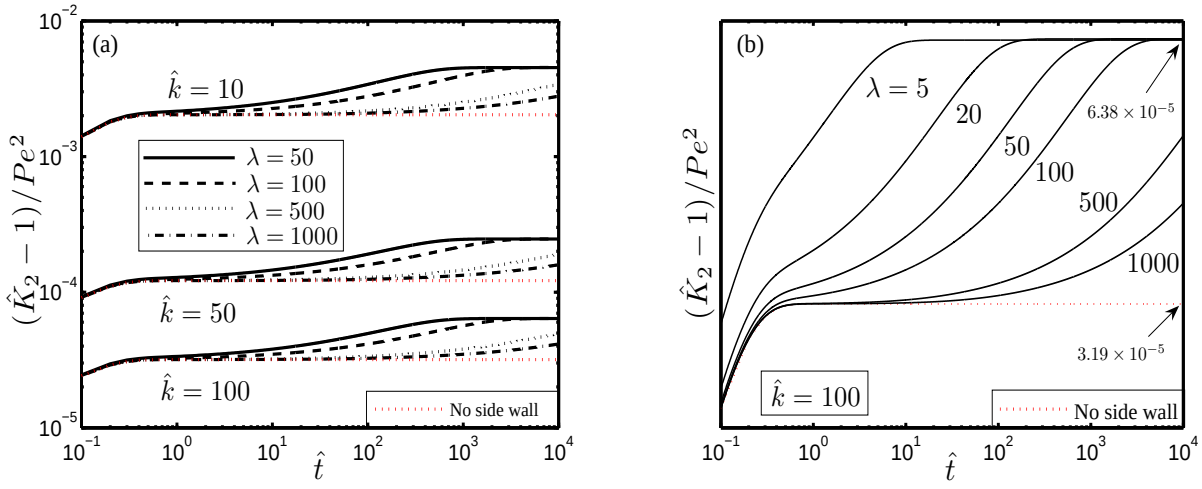

Figure 3: (a) The numerical factor of the dispersion coefficient, $(\hat{K}_2 - 1)/Pe^2$, as a function of the dimensionless time, $\hat{t} = tD/h^2$, for different values of the aspect ratio λ and the Debye–Hückel parameter $\hat{k}$; (b) a magnified view of the curves corresponding to $\hat{k} = 100$. The dotted lines are for the corresponding parallel-plate channel.

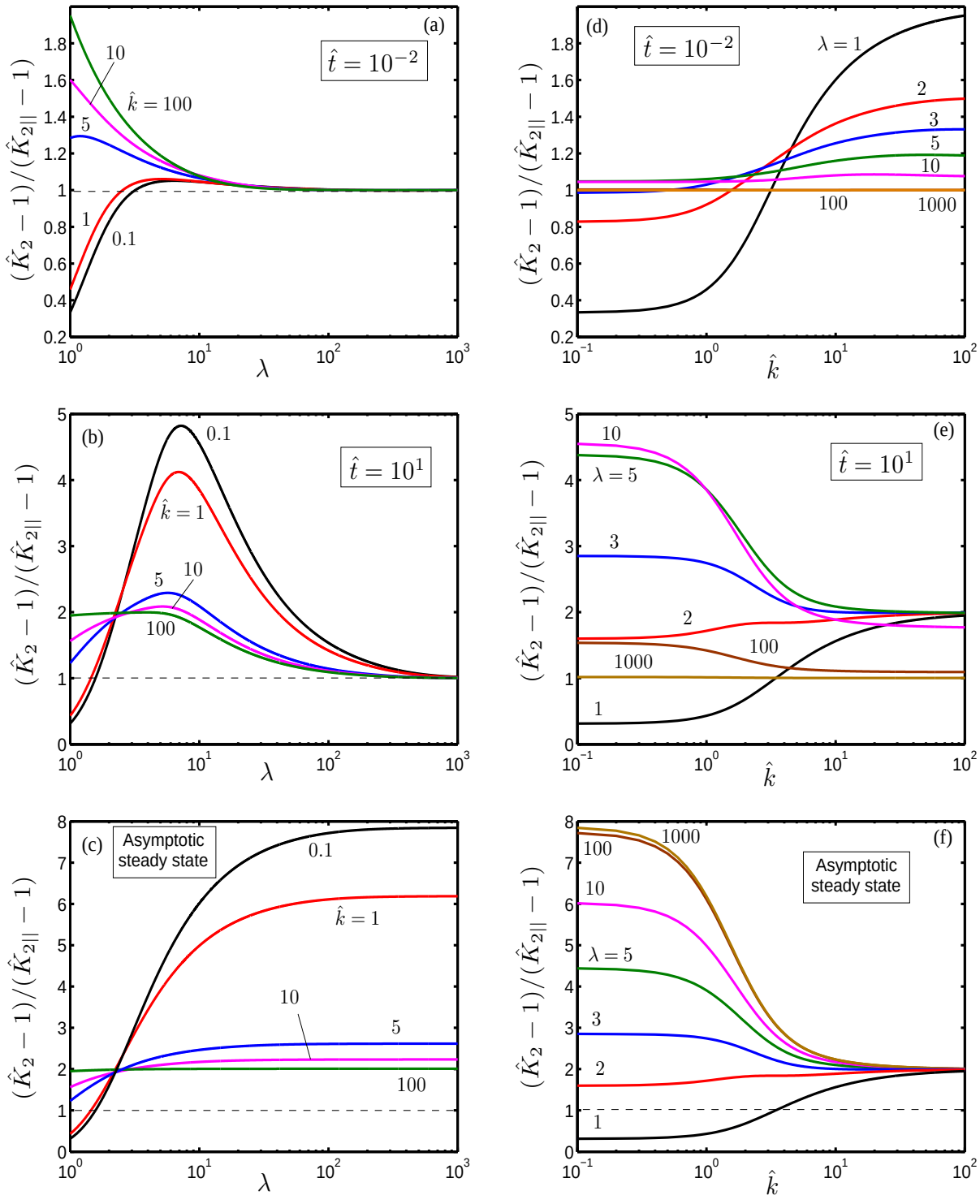

Figure 4: The ratio of the numerical factors of the dispersion coefficients for the two geometries, $(\hat{K}_2 - 1)/(\hat{K}_{2\|} - 1)$, at different times: (a, b, c) as a function of the aspect ratio λ for different values of the Debye–Hückel parameter $\hat{k}$; (d, e, f) as a function of the Debye–Hückel parameter $\hat{k}$ for different values of the aspect ratio λ.